NUCL SCI TECH (2020) 31:96
https://doi.org/10.1007/s41365-020-00807-5

Characterization of metal element distributions in the rat brain following ischemic stroke by synchrotron radiation micro-fluorescence analysis

Shu-Peng Shi[1] · Hui Wang[1] · Zhuo-Hui Chen[1] · Xiao-Han Li[1] · Shi-Xin Liu[1] · Meng-Qi Zhang[1,2]

Received: 24 April 2020 / Revised: 16 August 2020 / Accepted: 20 August 2020 / Published online: 1 October 2020
© China Science Publishing & Media Ltd. (Science Press), Shanghai Institute of Applied Physics, the Chinese Academy of Sciences, Chinese Nuclear Society and Springer Nature Singapore Pte Ltd. 2020

Abstract Ischemic stroke is one of the leading causes of death worldwide, and effective treatment strategies in the chronic phase of this disease remain insufficient. Homeostasis of metals in the brain plays an important role in maintaining normal brain function. However, the dynamic spatial distributions of iron, zinc, calcium, potassium, and copper in a rat brain following ischemic stroke and the association between structural distribution and function remain to be elucidated. In this study, we used a synchrotron radiation-based micro-X-ray fluorescence technique to image element mapping changes in special rat brain regions after ischemic stroke, showing the distribution characteristics of iron, zinc, calcium, potassium, and copper. We demonstrated, for the first time, the consistent dynamic spatial distributions of metal elements at a series of time points (3 h, 4.5 h, 6 h, 12 h, 1 d, 3 d, 5 d, 7 d, 10 d, 14 d, 28 d) after brain ischemia, which revealed that the homeostasis of iron, zinc, calcium, potassium, and copper in the brain was disturbed with distinctive change trends, providing clear insights in understanding the underlying pathogenesis of stroke from a novel perspective, thus laying the foundation of further developing new drug targets for stroke treatment.

Keywords Ischemic stroke · Synchrotron radiation · X-ray fluorescence · Metal · Rat brain

1 Introduction

Metal elements, rich in coordination chemistry and redox properties, are effectively stored, released, and utilized by cells and tissues to form or enhance the structure and function of proteins and carry out vital life processes [1]. In the human body, the central nervous system, which is the command center for cognitive and motor functions, has immense biological complexity and contains several endogenous complexes that are involved in signaling, biosynthesis, and metabolic processes [2]. Metal elements play a particularly important role during some specific neurobiological processes, and their distributions in the brain are closely linked with diseases [3–5]. Although some structural features of the brain have been illustrated, the spatial distributions of its critical elements have not been entirely elucidated. As the element spatial distribution is usually uneven in different regional structures [6, 7], functional imaging to localize critical elements in specific tissues is important to determine their metabolic and physiological roles. Therefore, it is of great significance to investigate the spatial distribution of critical elements in the brain under physiological and various pathological conditions.

Traditionally, element analyses of biological samples have been based on destructive methods leading to the loss

Shu-Peng Shi, Hui Wang, and Zhuo-Hui Chen contributed equally to the work described in this paper.

This work was supported by the National Natural Science Foundation of China (No. 81501025) and the Natural Science Foundation of Hunan Province (Nos. 2020JJ4134 and 2016JJ3174).

✉ Meng-Qi Zhang
zhangmengqi8912@163.com

[1] Department of Neurology, Xiangya Hospital, Central South University, Changsha 410008, China

[2] National Clinical Research Center for Geriatric Disorders, Xiangya Hospital, Central South University, Changsha 410008, China

of information about the element spatial distribution within the tissue. In particular, even the amount of some elements in organisms is significantly low for current traditional methods to investigate due to the lack of relatively high spatial resolution and sensitivity [8]. Several technologies based on mass spectrometry have been developed to visualize the elements of biological samples including laser ablation inductively coupled plasma mass spectrometry (LAICPMS), time-of-flight secondary ion mass spectrometry (TOF-SIMS), and nanoscale secondary ion mass spectrometry (NanoSIMS). However, each of these imaging techniques has several disadvantages in detecting the element distribution, specifically in metal detection. The most essential drawback of these methods is the destruction of samples since the methods need to sputter the surface material of the sample for composition analysis [9–12]. The spatial resolution of LAICPMS is relatively limited, prohibiting the realization of elemental analysis at a subcellular level [10]. Due to its rather high matrix effect on molecular ion formation, it is difficult to quantify the elemental content/distribution using TOF-SIMS, thus making this technique more suitable for small organic molecules such as lipids [9]. Regarding NanoSIMS, limited secondary ion species (up to seven) can be achieved in one scan, impeding the application in the multielement analysis [11]. Thus, it is highly desirable to develop a novel imaging technology with high resolution that can visualize the spatial distribution of elements nondestructively. With the advent of third-generation synchrotron radiation (SR) light source, SR-based micro-X-ray fluorescence analysis (SR-μXRF) is available for nondestructive detection of elements in the femtogram range at the micrometer or even nanometer level [8]. Additionally, the elements of biological interest can be simultaneously detected in situ and mapped by SR-μXRF [13]. At present, SR-μXRF technology is applied in a wide range of scientific fields, such as geochemistry, astrochemistry, environmental science, and materials science [14–16].

As is well known, stroke is characterized by high incidence, high mortality, high morbidity, and a high recurrence rate due to acute cerebral circulation disorders. Particularly, ischemic stroke is currently one of the three major causes of death [17]. Studies have shown that brain ischemia can cause endogenous angiogenesis, a vital self-compensatory mechanism [18]. The extent of vascular proliferation is directly related to the improvement of blood flow in ischemic brain regions, affecting the recovery of neuronal physiological function [19]. Promoting angiogenesis has become one of the important strategies in stroke treatment and rehabilitation. Finney et al. used SR-μXRF to image the distribution of metal ions in microvascular endothelial cells and showed that copper (Cu), iron (Fe), zinc (Zn), and other elements changed with cell growth and cell redistribution, and gradually approached the growth points to be excreted outside the cell [20]. However, the above studies on ions and angiogenesis are limited to normal cell models. At the level of cells and animal models, the detailed distribution and concentration of vital metal ions such as Fe, Zn, and other metals in the process of angiogenesis after cerebral ischemia have not been reported up to now. Therefore, accurate qualitative and quantitative analysis of the ion imbalance in the process of cerebral ischemia and its mechanism is needed to further understand the occurrence and development of stroke and is expected to provide a new perspective of stroke therapy.

This study is proposed to establish rat models of middle cerebral artery occlusion (MCAO) with a series of ischemic time courses and subsequently to characterize the spatial distributions of metal elements in focal functional brain regions by SR micro-beam X-ray fluorescence imaging technology. These findings will provide new insights into the distribution of elements under ischemic conditions, thereby providing a promising tool for the evaluation of brain ischemic injury repair.

2 Materials and methods

2.1 Sample preparation

The experiment was conducted in the Experimental Zoology Department of Central South University, Changsha, China, and was in line with Central South University experimental welfare ethics review standards. Male Specific Pathogen Free (SPF) *Sprague–Dawley rats* weighing 250–280 g were used for establishing models and provided by Laboratory Animal Center of Central South University. The intraluminal suture method [2] was used to establish stroke rat models with the right middle cerebral artery (MCA) occlusion, that is, the median anterior cervical incision first, and then exposing the right common carotid artery bifurcation, inserting a standard nylon thread from the common carotid artery near the bifurcation into the internal carotid artery with a depth of approximately 18 ± 0.5 mm. According to the description of Longa et al., neurobehavioral experiments were performed immediately after surgery in rats to evaluate the effect of occlusion [21]. Following the principle of random allocation, 48 rats were randomly assigned to 12 groups, including the sham operation group and groups with occluded right middle artery for 3 h, 4.5 h, 6 h, 12 h, 1 d, 3 d, 5 d, 7 d, 10 d, 14 d, and 28 d, respectively, based on duration of occlusion. During the feeding period, 1 rat in the 10 d group, 2 rats in the 14 d group, and 2 rats in the 28 d group died of a stroke. To ensure that at least 3 rats were involved in each group, a

total of 2 rats were randomly added into the 14 d and 28 d groups. In total, 50 rats were used and 45 were included in our study. After removing the intraluminal suture from the 45 successful models, the models were anesthetized and subsequently sacrificed by perfusing with 0.9% saline and ice-cold paraformaldehyde successively. The separated intact brain was fixed with paraformaldehyde in 0.1 M phosphate-buffered saline (pH 7.4) overnight and subsequently dehydrated in 30% sucrose for 24 h. The most successful brain samples were collected in each group, with the principle of complete perfusion, no visible blood remaining, and a rather stiff surface. The collected sample was immediately frozen and was subsequently sectioned in the coronal plane using a cryostat to obtain ten 60-μm-thick slices (containing the hippocampus). For analysis by SR-μXRF, the samples were finally dried in air to a fully dehydrated state and placed on 3-μm-thick Mylar membrane. To reduce errors, the entire sample preparation process was strictly regulated to avoid contamination with Fe, Zn, calcium, magnesium, and Cu.

2.2 Synchrotron radiation-based micro-X-ray fluorescence analysis (SR-μXRF)

SR-μXRF combines fluorescence X-ray analysis and X-ray microscopy. Fluorescence analysis is based on the X-ray fluorescence generated by the photoelectric effect of the interaction between the X-ray and the substance, and the information of the sample is analyzed. The photoelectric effect is observed when the photon energy of X-rays is greater than the electron binding energy of the object atoms. After absorbing the photon energy, the inner electron of the atom is finally transferred to the high energy level orbit, and the electron of the outer layer transfers to the electron hole of the inner layer to generate a fluorescent signal [2]. Therefore, within a certain range of X-ray photon energies, the fluorescence signals emitted by different elements are different according to the different electron binding energy and electron arrangement of each elemental atom [1, 22]. In this experiment, the scanning analysis of the distribution of Fe, Zn, calcium, magnesium, and Cu in the brain tissue by SR-μXRF was performed at beamline 15U station in Shanghai Synchrotron Radiation Facility (SSRF, Shanghai, China). The semiquantitative experiment was performed in air at room temperature with a photon energy of 10 keV and a monochromator angle of 45 degrees. The spot size of the beam on the sample stage was $50 \times 50\ \mu m^2$, with a focusing time of 1 s per point, a step size of 50 μm for raster scanning, and a silicon detector for collecting fluorescence counting of 90 degrees. A light microscope was coupled to a computer for sample viewing. Each pixel was extracted from the energy-dispersive spectrum using the GeoPIXE software (CSIRO, Australia), and the intensity map of the metal was imaged using Igor Pro software (WaveMetrics, USA) to quickly and accurately obtain two-dimensional, in situ micro-amounts of brain tissue element content and distribution. In experiments, Compton scattering in X-ray spectra was used as an internal standard to compensate for the differences in thickness and density between the thin sections of tissue.

2.3 Data analysis

Due to the high heterogeneity of elemental distribution in the brain-wide scale, the relative signal value of all the scanning spots (containing all the duplicate samples) was collected from the control side and the experimental side of the brain, thus dividing the data into two parts. Statistical analysis was performed using the Statistical Package for the Social Sciences version 20.0 (International Business Machines Corp., Armonk, NY). A nested *t* test was conducted to compare the difference between the sham group and different post-MCAO time point groups. $P < 0.05$ was considered to be significantly different. Data are presented as the mean ± standard deviation (SD).

3 Results

The contents and distribution images of Fe, Zn, Ca, K, and Cu in rat brain tissues were obtained by SR-μXRF. The images change gradually during the progression of ischemia.

3.1 Iron fluorescence mapping

According to the image (Fig. 1), the distribution of Fe element in the sham group was more even and the average value was higher in the vicinity of the cortex. However, in the cerebral ischemia group, the average value of Fe was higher in the cortex and lesion area. The content of Fe in the lesion area evidently increased early and subsequently decreased over time. In the short-duration groups, the mean value at 3 h increased and slightly decreased at 4.5 h and 6 h, and distribution means at 12 h and 1 d increased in the local region, specifically in the lesion area. In the long-duration groups, the content of Fe element in 1 d to 5 d showed a recovering and decreasing trend and in 7 d–14 d continued to decrease to a smaller volume of lesion hemisphere. In the long-duration experimental groups, the fluctuation of Fe in the continuously perfused left brain tissue region was not evident when compared to the lesion side, i.e., side with interrupted blood supply.

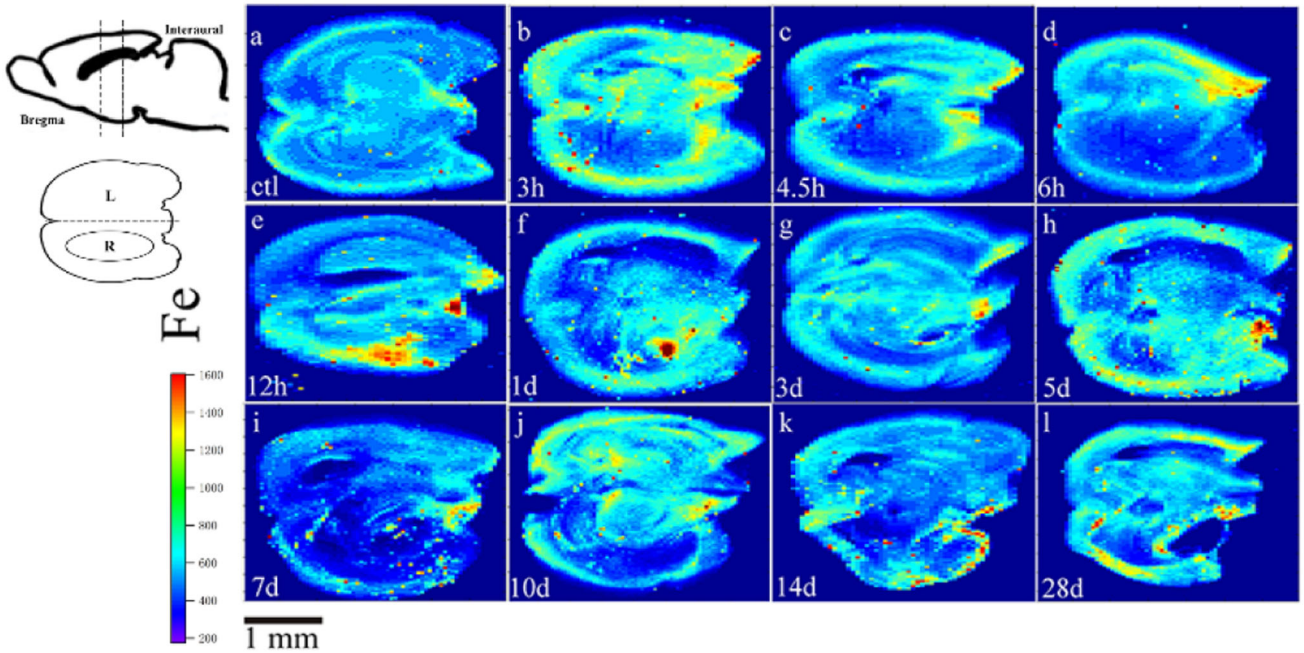

Fig. 1 (Color online) Image of iron (Fe) distribution in the brain tissues at different post-middle cerebral artery occlusion (MCAO) time points by synchrotron radiation-based micro-X-ray fluorescence analysis. **a** Fe distribution in brain tissue of sham-operated rat. **b–l** Fe distribution in rat brain tissue at post-MCAO 3 h, 4.5 h, 6 h, 12 h, 1 d, 3 d, 5 d, 7 d, 10 d, 14 d, and 28 d, respectively. The sagittal plane of a rat brain demonstrated the position from which the slice was obtained. The ischemic lesion was on the right hemisphere marked with "R"

3.2 Zinc fluorescence mapping

According to the image (Fig. 2), Zn distribution in the sham group was average compared to the other groups, and the mean was lower, while Zn in the cerebral ischemia group was not evenly distributed. In the short-duration groups, the distribution of Zn was more balanced, and the mean elemental content was higher than that in the sham group. In the long-duration groups, the means of Zn in the lesion area fluctuated over time. The results showed that the Zn content in the 1d group increased, after which the Zn content in the 5 d group increased and exceeded that in the 3 d group. Subsequently, in the 7 d group, the Zn content decreased, and the Zn content in the 14 d and 28 d groups decreased successively. The Zn content in 28 d group was significantly low, specifically in the center of the lesion. In contrast, the fluctuation of the Zn content on the normal side was small.

3.3 Calcium fluorescence mapping

According to the image (Fig. 3), the distribution of Ca in the sham group was more balanced, and its distribution in the cerebral ischemia group was unbalanced. The distribution of Ca was mainly on the lesion side. In the long-duration groups, the content continued to increase, and the highest content was observed in the 28 d samples. In the short-duration groups, the means and distribution of Ca did not have significant change compared with the sham group. However, the means and distribution of Ca seemed to increase slightly in the lesion area, which was close to the 1d group. The means of Ca content in the normal side were all lower than that in the lesion side in the same sample.

3.4 Potassium fluorescence mapping

According to the image (Fig. 4), the distribution of K in the sham group was more even. In the experimental group (3 h, 4.5 h, 6 h, 12 h), the average values of K decreased slightly, and the distribution did not have significant changes compared with the sham group. Over time, the means of K increased significantly on the lesion side in the 1d group and decreased again in the 3 d group. The content of cortex K in the 5 d, 7 d, 10 d, 14 d, and 28 d groups showed a slight increase when compared with the ahead groups, with distribution seen on the lesion areas, while the content in the lesion core area (striatum) was still relatively low. However, compared with the other elements, the increasing degree of means in every group was not significantly high.

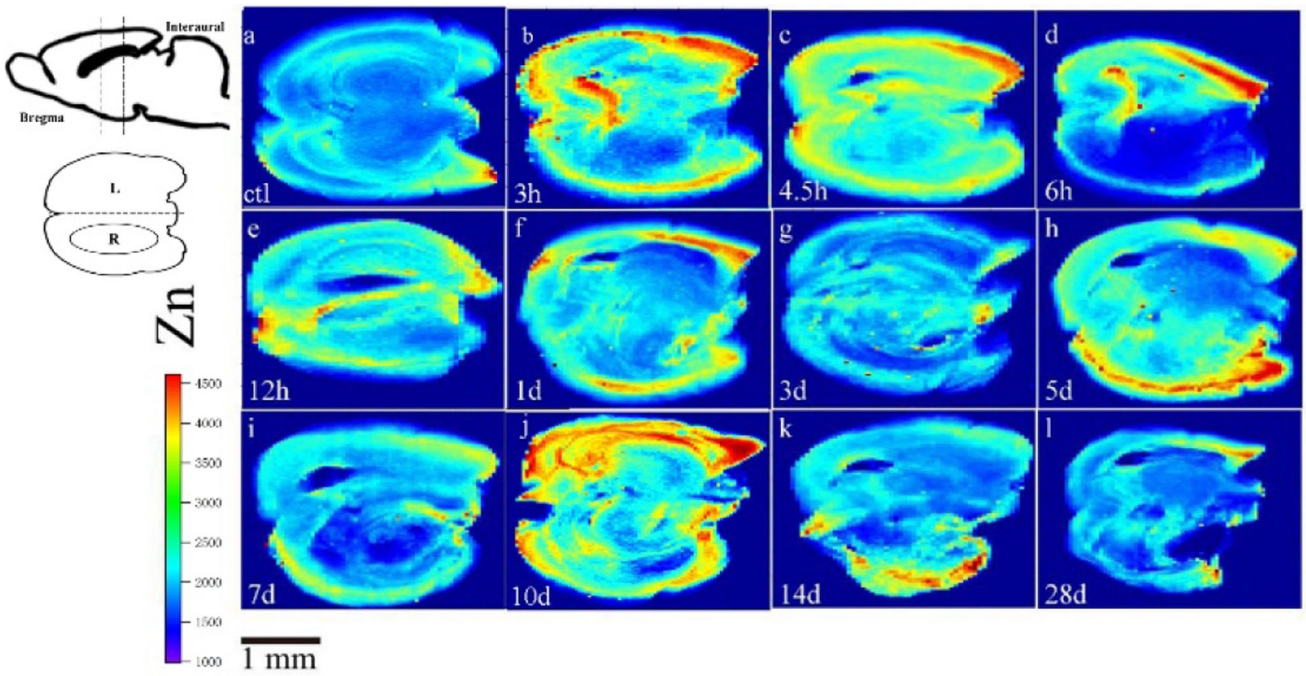

Fig. 2 (Color online) Image of zinc (Zn) distribution in the brain tissues at different post-middle cerebral artery occlusion (MCAO) time points by synchrotron radiation-based micro-X-ray fluorescence analysis. **a** Zn distribution in brain tissue of sham-operated rat. **b–l** Zn distribution in rat brain tissue at post-MCAO 3 h, 4.5 h, 6 h, 12 h, 1 d, 3 d, 5 d, 7 d, 10 d, 14 d, and 28 d, respectively. The sagittal plane of a rat brain demonstrated the position from which the slice was obtained. The ischemic lesion was on the right hemisphere marked with "R"

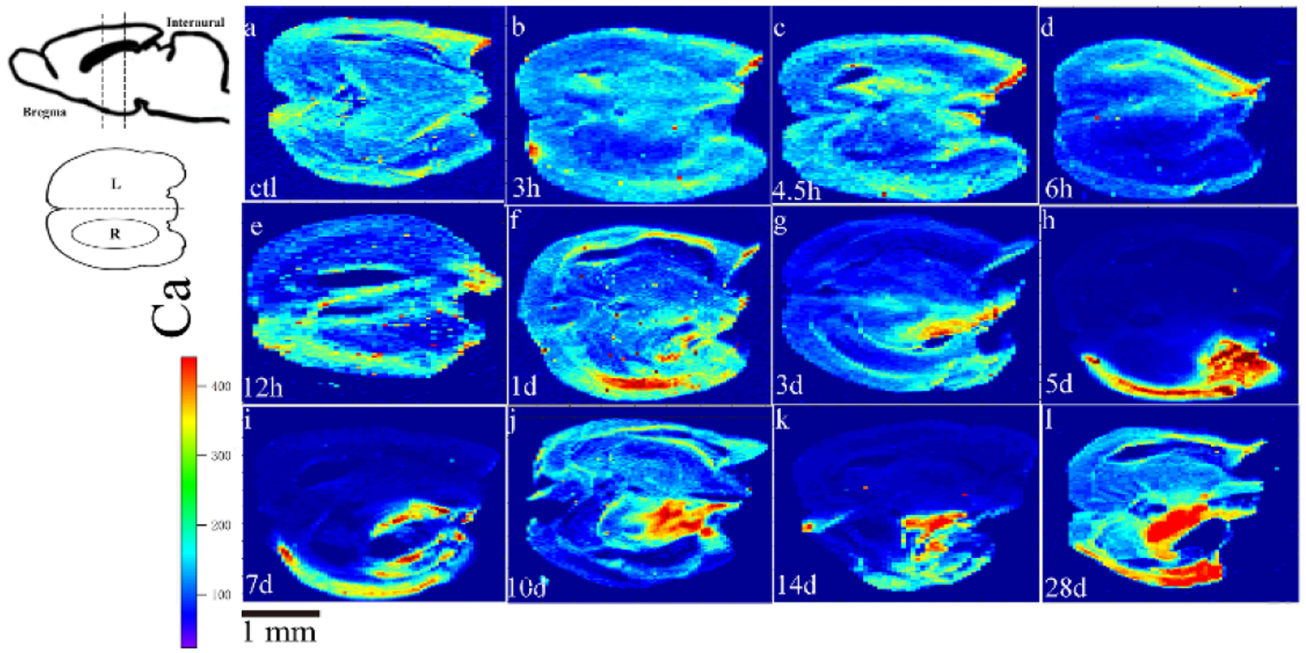

Fig. 3 (Color online) Image of calcium (Ca) distribution in the brain tissues at different post-middle cerebral artery occlusion (MCAO) time points by synchrotron radiation-based micro-X-ray fluorescence analysis. **a** Ca distribution in brain tissue of sham-operated rat. **b–l** Ca distribution in rat brain tissue at post-MCAO 3 h, 4.5 h, 6 h, 12 h, 1d, 3 d, 5 d, 7 d, 10 d, 14 d, and 28 d, respectively. The sagittal plane of a rat brain demonstrated the position from which the slice was obtained. The ischemic lesion was on the right hemisphere marked with "R"

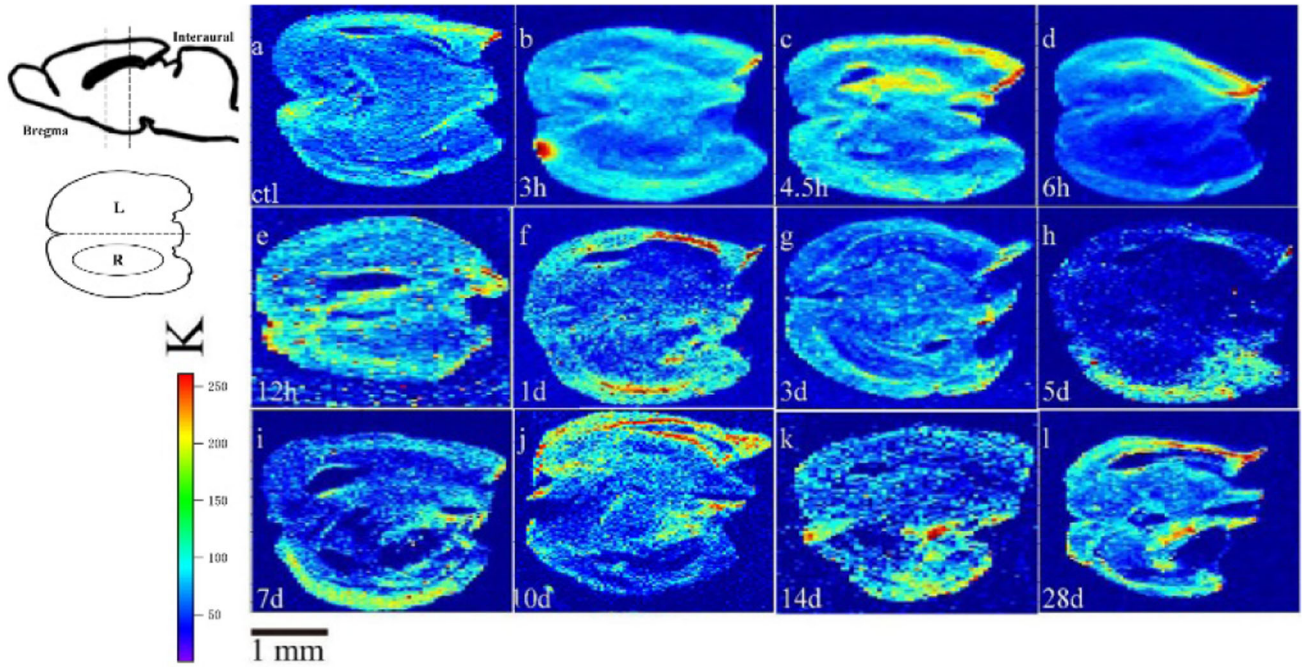

Fig. 4 (Color online) Image of potassium (K) distribution in the brain tissues at different post-middle cerebral artery occlusion (MCAO) time points by synchrotron radiation-based micro-X-ray fluorescence analysis. **a** K distribution in brain tissue of sham-operated rat. **b–l** K distribution in rat brain tissue at post-MCAO 3 h, 4.5 h, 6 h, 12 h, 1d, 3 d, 5 d, 7 d, 10 d, 14 d, and 28 d, respectively. The sagittal plane of a rat brain demonstrated the position from which the slice was obtained. The ischemic lesion was on the right hemisphere marked with "R"

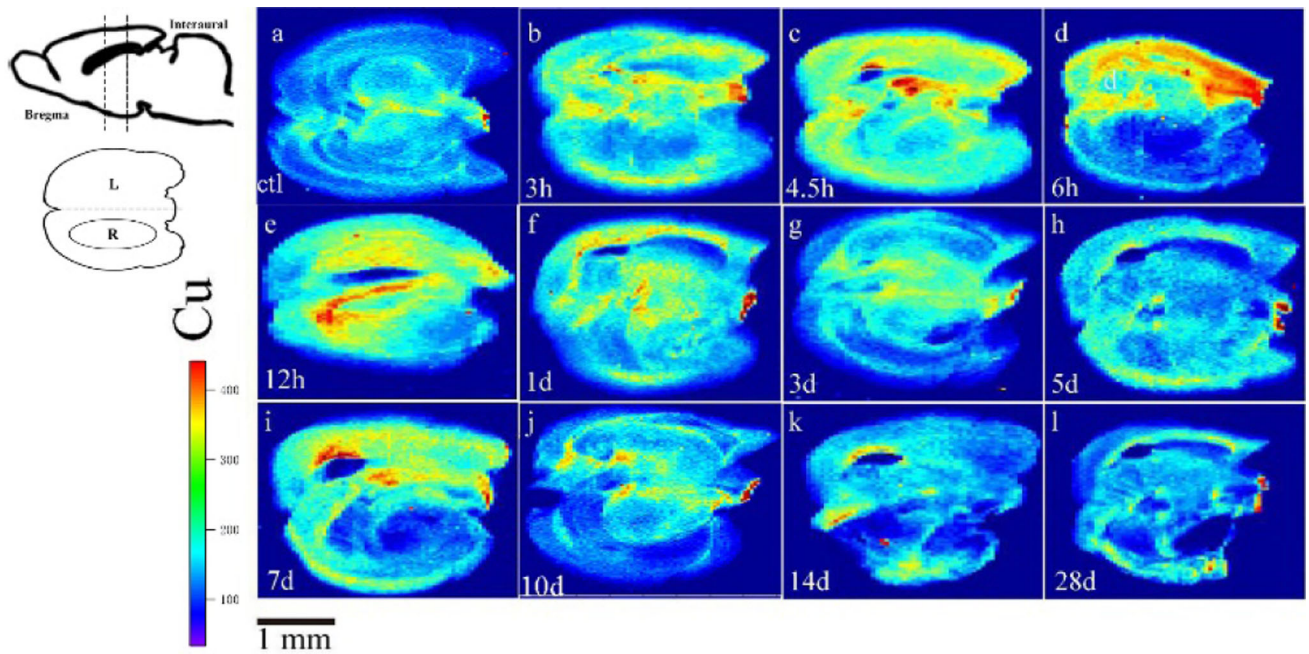

Fig. 5 (Color online) Image of cupper (Cu) distribution in the brain tissues at different post-middle cerebral artery occlusion (MCAO) time points by synchrotron radiation-based micro-X-ray fluorescence analysis. **a** Cu distribution in brain tissue of sham-operated rat. **b–l** Cu distribution in rat brain tissue at post-MCAO 3 h, 4.5 h, 6 h, 12 h, 1 d, 3 d, 5 d, 7 d, 10 d, 14 d, and 28 d, respectively. The sagittal plane of a rat brain demonstrated the position from which the slice was obtained. The ischemic lesion was on the right hemisphere marked with "R"

3.5 Copper fluorescence mapping

According to the image (Fig. 5), in the sham group, the mean of Cu was higher around the median sagittal line. In the short-duration group (3 h, 4.5 h, 6 h, 12 h, and 1 d), the expression of Cu increased extensively in the brain tissue of the experimental groups. From the 3rd day, the overall Cu content decreased, and the lesion side was lower than the control side.

3.6 Quantitative analysis

To quantitatively evaluate the difference between the sham group and the several post-MCAO time point groups, we collected the relative signal value of the elements from all the scanning spots due to the high heterogeneity of the data in the brain-wide scale. The collected data were subsequently divided into two parts, the control side and the experimental side, to take into account the different conditions endured by the two brain hemispheres. The data were presented using a histogram (Fig. 6). The statistical evaluation showed a high SD value in almost all the groups and confirmed the heterogeneity of element distribution in the brain. In the whole-brain scale, the content of Fe, Ca, and Cu was relatively stable after MCAO operation, although the local change was significant (Figs. 1, 3, 5). It also indicated that K and Zn changed more significantly than other elements during the progression of MCAO. The content of K changed significantly in almost all the time points after MCAO, and Zn mainly changed after 3 d.

4 Discussion

The research on the spatial distribution and concentration of metals in the brain only focused on a short period since the onset of ischemic stroke. Takahashi et al. studied the changes in brain elements after MCA occlusion for 3 h and 24 h and found that the changes had no significant difference [23]. Our experiment added more intervals (from 3 h to 28 d). Element distribution mapping of various metal elements at specific sites was obtained by SR-μXRF, indicating the dynamic enrichment process during focal ischemic stroke, providing a basis to explore the variation of metal element contents and functions during the stroke process, for further research on new drug targets.

With different occlusion time of the MCA, the pathophysiological changes in brain tissue are different and change over time. Therefore, the contents and distributions of metal elements at different time points and changes in pathophysiology in each step of the process are tightly associated. At present, the mechanism underlying the imbalance in metal element homeostasis after ischemia remains to be elucidated.

4.1 Iron

Fe, one of the essential elements in the body, is a prosthetic group of neurotransmitters and important myelin protein synthase. Fe ion is also a catalyst that significantly increases the concentration of reactive oxygen species (ROS). Studies have shown that after Fe aggregation, a

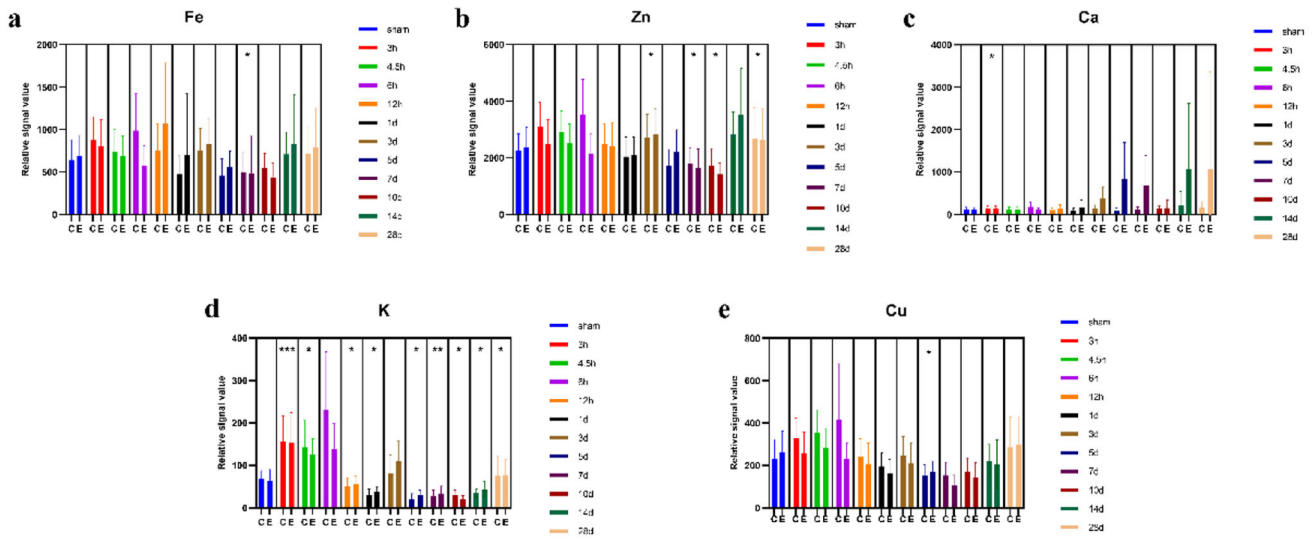

Fig. 6 (Color online) Quantification of the relative signal value of various elements at different post-middle cerebral artery occlusion (MCAO) time points. **a–e** The quantification of iron, zinc, calcium, potassium, and copper on the control side and experimental side of the brain at different time points after MCAO. "C" and "E" represent the control side and experimental side, respectively. Nested *t* test was employed to test the difference between the post-MCAO groups and the sham group on the whole-brain scale. $*P < 0.05$, $**P < 0.01$, $***P < 0.001$ versus the sham group at each time point

large number of hydroxyl radical generated by Fenton reaction can promote the peroxidation of membrane lipid and the production of ROS, leading to cytotoxic damage. Studies have found that neurons have Fe ion metabolism disorders in Alzheimer's disease (AD) [24]. The activation of nuclear factor kappa-light-chain-enhancer of activated B cells leads to increasing divalent metal transporter 1 expression, increasing Fe influx, and aggravating neuronal damage after cerebral ischemia [25]. Moreover, with cerebral hemorrhage, hemoglobin degrades to heme Fe, thereby promoting the production of ROS [26]. Furthermore, intravenous injection of Zn (2+) into Wistar rats can reduce the Fe accumulation after cerebral ischemia, which can cause neuronal damage, and the Fe chelator deferoxamine can reduce the severity of myocardial infarction induced by Fe aggregation after cardiac ischemia–reperfusion [27]. Studies have shown that there are two main sources of Fe in the lesion area: (1) hypoxia–ischemia that damages the blood–brain barrier and the free Fe ions that directly leak into the brain instead of through the involvement of transferrin, and (2) ischemia leads brain cells to reduce the regulation of Fe storage protein, resulting in increased concentration of free Fe ions in the brain tissue. In hypoxic conditions, the free ferric ions are reduced to ferrous ions, and the ferrous ions undergo Haber–Weiss reaction to generate hydroxyl radicals, resulting in oxidative stress and subsequent cell apoptosis and tissue infarction [23, 28, 29]. Moreover, some studies have shown that the protection of the blood–brain barrier after ischemic stroke and the use of some lipid-soluble Fe chelators can reduce the infarct range and ROS production [30].

Fe content of lesions in elemental distribution map increased first and subsequently decreased, which suggests that ischemic brain tissue oxidative stress response increased first, and compensatory repair was subsequently observed. Recent studies have found that prophylactic knocking out of the Tau gene that mediates Fe export has protective benefits on brain tissues after MCAO [31]. Combined with our results, they jointly imply that early clinical intervention to increased local Fe content is of great importance.

4.2 Zinc

Various studies have shown that during cerebral ischemia, Zn has the dual role of neurotoxicity and neuroprotection. Selective death of hippocampi 1 neurons during cerebral ischemia is caused by the release of Zn-containing vesicles at the terminal axon of excitatory neurons to fragile postsynaptic neurons [32]. Zn can affect adenosine triphosphate consumption and the oxidized form of coenzyme NAD^+ to disrupt the different phases of cellular respiration. Moreover, the use of Zn chelators reduces neuronal death [33, 34]. Successive studies have shown that in the early stages of ischemia, vulnerable neurons upregulate the expression of Zn transporter protein-1 (a local plasma membrane transport protein that promotes Zn efflux). However, contrary to chelation-based therapeutic interventions, various studies have demonstrated the neuroprotective benefits following various Zn compounds [35]; hence, Zn should have neurotoxic and neuroprotective dynamic balance in a postischemic setting. It is hypothesized that this may be related to the fluctuation of Zn content distribution in postischemic lesions (the specific changes are shown in the experimental results).

4.3 Calcium

The mechanism of Ca ion cytotoxicity is still controversial. There are mainly intracellular "calcium overload" hypothesis and "source-specific" hypothesis, both of which are related to the entry of calcium ions from the extracellular and endoplasmic reticulum, mitochondria, into the neurons' cytoplasm after cerebral ischemia. As a neurotransmitter, glutamate develops excitotoxicity in ischemic environment. It can overstimulate receptors such as *N*-methyl-D-aspartic acid receptor (NMDA) and allow a large influx of Ca ions [36, 37]. Studies have shown that the use of NMDA receptor blocker BQ-869 can reduce intracellular Ca concentration and reduce the infarct range of the tissue [38]. Membrane disintegration of the endoplasmic reticulum and mitochondria or dysfunction of membrane ion channels releases Ca into the cytoplasm [36]. Increased intracellular free Ca has become an important cause of cell death. With the extension of time, in the elemental distribution map, the lesion areas have high Ca content, specifically in the 28 d group. It has been hypothesized that this distribution may be related to the formation of calcification, which may be related to ischemic necrosis and increased alkaline phosphatase of the local tissue.

4.4 Potassium

Some studies have shown that during the edema phase of the ischemia, the blood–brain barrier is destroyed, Na ions flow in, and K ions flow out in large quantities [39]. The change of Na and K ions inside and outside the neurons contributed to pure cytotoxic edema in the ischemic hemisphere [40, 41]. This may be related to the early reduction of the K content in the lesion areas of the element distribution map. This is consistent with Sentaro et al.'s findings. The blockade of K-related ion channels plays an important role in controlling neuronal hyperactivity after ischemia [42]. Ischemic stroke accounts for a higher risk of epileptogenesis [43], which may also be highly connected

with K and cortical spreading depolarization. Compared to the control groups without post-stroke epilepsy, the post-stroke epilepsy group showed a significant reduction in Kv4.2, a type AK channel subunit [44]. Additionally, cortical spreading depolarization and epilepsy often occur simultaneously after ischemic stroke. The interplay between cortical spreading depolarization and epilepsy is also complicated. The contradiction of which one initiates the other electrophysiological phenomena still existed [45]. It has the potential to alter the threshold of epileptogenesis by manipulating the occurrence of cortical spreading depolarization, which may reduce the epilepsy-associated sequelae [46]. Furthermore, serum potassium levels significantly affect the prognosis of ischemic stroke patients [47]. In the elemental distribution map, the content of the lesion core is lower, while the cortex and around the lesion core shows an increasing trend, which could be, respectively, explained by the flow out theory and compensatory theory.

4.5 Copper

Cu is a strong oxidant, and its effects include phospholipid synthesis, hemoglobin formation, and electron transport. Cu is a trace element necessary for several key processes in the brain [48]. Although studies of chronic neurodegenerative diseases such as AD have shown that Cu homeostasis of the brain has been disturbed, little is known about Cu homeostasis of brain tissue in acute ischemic stroke. Recent studies indicate that Cu transmission plays an important role in the regulation of immune response in the brain. CuII (atsm), a type of Cu bis (thiosemicarbazone) complex, reduces the damage of the postischemic immune response to the brain tissue by influencing the immunogenic effects of several cells and activity of microglia [49, 50], which has a great potential for the treatment of ischemic stroke. In the elemental distribution map, the changing trend of Cu in lesions after cerebral ischemia is similar to that of Fe; thus, the oxidative stress reaction caused by Fe element may be correlated with the immune response of Cu, increasing and decreasing synchronously.

By SR-μXRF, this experimental result showed that after an ischemic stroke, the in situ steady state of Fe, Zn, Ca, K, and Cu in brain tissue is imbalanced. Combined with previous research results, the changes in these elements aim to provide a new idea and target for the study of ischemic stroke intervention. For the early increase in Fe content, clinical intervention should be performed as soon as possible, or intervention of patients with stroke prognosis should be performed in advance, to avoid a series of oxidative damages of Fe after stroke. The content of Cu relatively presented a similar trend of fluctuation compared to Fe, that is, the initial increase and the following decrease in the content of the two elements. The specific association between Cu and Fe homeostasis in the human body is complicated; hence, dyshomeostasis of the two elements is observed. It has been reported that Fe concentration decreases after feeding a Cu-deficient diet in a rat model [51]. Interestingly, a similar changing trend of Cu and Fe has been observed in our results. However, it has also been reported that the lack of ceruloplasmin, a type of Cu-binding protein, causes Fe to accumulate in the pancreas, retina, and brain [52]. This indicated that in different pathological processes, the metabolism of Cu and Fe can vary greatly, even in the opposite manner. The exact association between the two elements in the brain remains elucidated, specifically after ischemic stroke. Thus, the research about which role Cu plays to Fe during ischemic stroke is significantly valuable. If there is certainly an antagonistic effect of Cu, this can provide a new target for the clinical treatment of stroke. The experiment also found that the content of potassium, consistent with the results of other studies, decreased early, after which it has slightly increased. Potassium is an important ion involved in the resting potential and action potential of the neuron. The specific mechanism of later increased change needs to be further explored.

The statistical analysis also provided interesting information about the progression of MCAO. It confirmed that the distribution of different elements was imbalanced because of a rather high SD value in almost every group. Additionally, the nested *t* test was conducted to compare the difference of element content between the sham group and the different post-MCAO time point groups. The results showed that the content of potassium significantly changed in almost all the time point groups, specifically in the early phase of MCAO (3 h, 4.5 h, 12 h), indicating its essential role in initiating the pathology of ischemic stroke. Moreover, the content of Zn also changed significantly at the time points of 3 d, 7 d, 10 d, and 28 d, suggesting its important role in the later period of ischemic stroke. Regarding the shortage of our statistical analysis, the nested *t* test can only test the difference between the sham group and the experimental groups on a brain-wide scale and caused the neglect of the local information. For example, there are several "heat zones" and "cold zones" presented in Figs. 1, 2, 3, 4 and 5, indicating the local enrichment or depletion of these elements. Our results showed that the content of Fe and Ca did not change significantly in the whole-brain scale after the MCAO. Thus, the local enrichment of Fe and Ca may be related to the functional or pathological change of the corresponding encephalic region. Additionally, the hot spots in K and Zn images may be caused by both the functional change and the change of inflow or outflow of the elements in the brain. Due to the limited sample size in our present study,

further study that determines the exact association between these heat and cold zones and the functional change of specific encephalic regions should be conducted. We believed that this local information was also important to decipher the progression of ischemic stroke.

4.6 Future perspective of SR-μXRF

SR produces rather strong X-rays, which are several orders of magnitude higher in intensity than laboratory X-ray sources. It can focus on the micron or even nanometer scales and can be used to observe cellular or intracellular micro-element distribution [53, 54]. Considering its nondestructive feature to the biological tissue, the SR-μXRF method used in the analysis of metal elements in biological tissues is considered as one of the most reliable methods for quantitative and in situ analysis of trace elements in biological systems, providing strong technical support for some diseases, specifically of the nervous system [55]. However, several problems are still to be addressed to optimize the efficiency of the scanning using SR-μXRF, for instance, accelerating the acquisition process to increase data acquisition efficiency and developing smaller beam sizes to enhance resolution without reducing the visual field [56]. Additionally, the radiation damage also existed during the scanning, which should be avoided by choosing proper scanning parameters. Previous studies have mentioned significantly possible utilization that may accelerate the finding of targets. For example, Epaule et al. used SR-μXRF technology to detect and map the distribution of a nanoparticle-packaged drug and confirmed that SR-μXRF is sufficiently sensitive to achieve the results [57], which may also be used to detect the distribution of brain-targeted medicine. Another example is that Wang et al. combined the immunogold labeling and SR-μXRF to detect the distribution of certain proteins including APP and Aβ42 in the brain [3], which indicates that SR-μXRF has the potential to combine with other technologies to increase the types of detection targets. These results suggest that SR-μXRF has the potential to assist in cerebrovascular disease, including ischemic stroke, directly or indirectly. Similar to ischemic stroke in this study, the disruption of homeostasis after the onset of the disease is closely related to the successive pathophysiological processes in brain tissue, such as oxidative stress. When conducting in-depth studies in the future, we will use SR-based three-dimensional (3D) micro-fluorescence imaging combined with 3D micro-tomography of angioarchitecture methods to further explore the mechanism and correlation of metal element changes with the plasticity of microvascular networks following cerebral ischemia, thus providing new targets for effective intervention of stroke [58–60].

5 Conclusion

In general, our study displays the distribution mapping of Fe, Zn, Ca, K, and Cu in the progression of focal brain ischemia, respectively, and primitively. SR-μXRF technology with nondestructive, high spatial resolution, and high sensitivity of multi-elemental analysis provides a powerful tool for the imaging of trace elements in biological tissues. Dynamic changes in metal elements in the brain during the development of ischemic stroke will be of great significance to explore the mechanisms and treatments of ischemic stroke.

Acknowledgements The authors would like to thank the staff at the BL15U station of SSRF for their kind assistance during the experiments.

Compliance with ethical standards

Ethical approval All animal experiments were approved by the Experimental Zoology Department of Central South University and performed following Central South University experimental welfare ethics review standards on the use of animals in research.

References

1. J.F. Collingwood, F. Adams, Chemical imaging analysis of the brain with X-ray methods. Spectrochim. Acta. B **130**, 101–118 (2017). https://doi.org/10.1016/j.sab.2017.02.013
2. E.L. Que, D.W. Domaille, C.J. Chang, Metals in neurobiology: probing their chemistry and biology with molecular imaging (vol 108, pg 1517, 2008). Chem. Rev. **108**(10), 4328 (2008). https://doi.org/10.1021/cr800447y
3. H. Wang, M. Wang, B. Wang et al., Immunogold labeling and X-ray fluorescence microscopy reveal enrichment ratios of Cu and Zn, metabolism of APP and amyloid-beta plaque formation in a mouse model of Alzheimer's disease. Metallomics **4**(10), 1113–1118 (2012). https://doi.org/10.1039/c2mt20056b
4. H. Wang, M. Wang, B. Wang et al., The distribution profile and oxidation states of biometals in APP transgenic mouse brain: dyshomeostasis with age and as a function of the development of Alzheimer's disease. Metallomics **4**(3), 289–296 (2012). https://doi.org/10.1039/c2mt00104g
5. H.-J. Wang, M. Wang, B. Wang et al., Quantitative imaging of element spatial distribution in the brain section of a mouse model of Alzheimer's disease using synchrotron radiation X-ray fluorescence analysis. J. Anal. Atom. Spectrom. **25**(3), 328–333 (2010). https://doi.org/10.1039/b921201a
6. P. Zatta, D. Drago, P. Zambenedetti et al., Accumulation of copper and other metal ions, and metallothionein I/II expression in the bovine brain as a function of aging. J. Chem. Neuroanat. **36**(1), 1–5 (2008). https://doi.org/10.1016/j.jchemneu.2008.02.008
7. G. Robison, T. Zakharova, S. Fu et al., X-ray fluorescence imaging of the hippocampal formation after manganese exposure. Metallomics **5**(11), 1554–1565 (2013). https://doi.org/10.1039/c3mt00133d
8. V.L. Dressler, E.I. Müller, D. Pozebon, Bioimaging Metallomics Adv. Exp. Med. Biol. **1055**, 139–181 (2018). https://doi.org/10.1007/978-3-319-90143-5_7

9. C. Bich, D. Touboul, A. Brunelle, Biomedical studies by TOF-SIMS imaging. Biointerphases **10**(1), 018901 (2014). https://doi.org/10.1116/1.4901511
10. A. Sussulini, J.S. Becker, J.S. Becker, Laser ablation ICP-MS: application in biomedical research. Mass Spectrom. Rev. **36**(1), 47–57 (2017). https://doi.org/10.1002/mas.21481
11. J. Nuñez, R. Renslow, J.B. Cliff et al., NanoSIMS for biological applications: current practices and analyses. Biointerphases **13**(3), 03B301 (2017). https://doi.org/10.1116/1.4993628
12. J. Decelle, G. Veronesi, B. Gallet et al., Subcellular chemical imaging: new avenues in cell biology. Trends Cell Biol. **30**(3), 173–188 (2020). https://doi.org/10.1016/j.tcb.2019.12.007
13. J.K. Jeon, J.K. Kim, Track analysis of a synchrotron X-ray photoelectric nanoradiator by in situ fluorescence imaging of reactive oxygen species: comparative study of gold and iron oxide nanoparticles. J. Synchrotron Radiat. **25**(Pt 6), 1768–1773 (2018). https://doi.org/10.1107/S1600577518011396
14. G. Van der Snickt, K. Janssens, J. Dik et al., Combined use of synchrotron radiation based micro-X-ray fluorescence, micro-X-ray diffraction, micro-X-ray absorption near-edge, and micro-fourier transform infrared spectroscopies for revealing an alternative degradation pathway of the pigment cadmium yellow in a painting by Van Gogh. Anal. Chem. **84**(23), 10221–10228 (2012). https://doi.org/10.1021/ac3015627
15. U.E.A. Fittschen, G. Falkenberg, Trends in environmental science using microscopic X-ray fluorescence. Spectrochim. Acta. B **66**(8), 567–580 (2011). https://doi.org/10.1016/j.sab.2011.06.006
16. R. Pérez-López, F. Macías, M.A. Caraballo et al., Mineralogy and geochemistry of Zn-rich mine-drainage precipitates from an MgO passive treatment system by synchrotron-based X-ray analysis. Environ. Sci. Technol. **45**(18), 7826–7833 (2011). https://doi.org/10.1021/es201667n
17. R.V. Krishnamurthi, V.L. Feigin, M.H. Forouzanfar et al., Global and regional burden of first-ever ischaemic and haemorrhagic stroke during 1990-2010: findings from the Global Burden of Disease Study 2010. Lancet Glob. Health. **1**(5), e259–e281 (2013). https://doi.org/10.1016/S2214-109X(13)70089-5
18. F. Ma, A. Morancho, J. Montaner et al., Endothelial progenitor cells and revascularization following stroke. Brain Res. **1623**, 150–159 (2015). https://doi.org/10.1016/j.brainres.2015.02.010
19. G. Esquiva, A. Grayston, A. Rosell, Revascularization and endothelial progenitor cells in stroke. Am. J. Physiol. Cell Physiol. **315**(5), C664–C674 (2018). https://doi.org/10.1152/ajpcell.00200.2018
20. L. Finney, S. Mandava, L. Ursos et al., X-ray fluorescence microscopy reveals large-scale relocalization and extracellular translocation of cellular copper during angiogenesis. Proc. Natl. Acad. Sci. U. S. A. **104**(7), 2247–2252 (2007). https://doi.org/10.1152/pnas.0607238104
21. E.Z. Longa, P.R. Weinstein, S. Carlson et al., Reversible middle cerebral artery occlusion without craniectomy in rats. Stroke **20**(1), 84–91 (1989). https://doi.org/10.1161/01.str.20.1.84
22. J. Chwiej, A. Patulska, A. Skoczen et al., Various ketogenic diets can differently support brain resistance against experimentally evoked seizures and seizure-induced elemental anomalies of hippocampal formation. J. Trace Elem. Med. Biol. **42**, 50–58 (2017). https://doi.org/10.1016/j.jtemb.2017.04.002
23. S. Takahashi, S. Hatashita, Y. Taba et al., Determination of the spatial distribution of major elements in the rat brain with X-ray fluorescence analysis. J. Neurosci. Methods **100**(1–2), 53–62 (2000). https://doi.org/10.1016/s0165-0270(00)00231-4
24. J.-L. Liu, Y.-G. Fan, Z.-S. Yang et al., Iron and Alzheimer's disease: from pathogenesis to therapeutic implications. Front. Neurosci. **12**, 632 (2018). https://doi.org/10.3389/fnins.2018.00632
25. R. Ingrassia, A. Lanzillotta, I. Sarnico et al., 1B/(-)IRE DMT1 expression during brain ischemia contributes to cell death mediated by NF-κB/RelA acetylation at Lys310. PLoS ONE **7**(5), e38019 (2012). https://doi.org/10.1371/journal.pone.0038019
26. L. Goldstein, Z.-P. Teng, E. Zeserson et al., Hemin induces an iron-dependent, oxidative injury to human neuron-like cells. J. Neurosci. Res. **73**(1), 113–121 (2003). https://doi.org/10.1002/jnr.10633
27. Y. Liu, J. Liu, H. Liu et al., Investigation of cerebral iron deposition in aged patients with ischemic cerebrovascular disease using susceptibility-weighted imaging. Ther. Clin. Risk Manag. **12**, 1239–1247 (2016). https://doi.org/10.2147/tcrm.S107783
28. A. Saleh, M. Schroeter, A. Ringelstein et al., Iron oxide particle-enhanced MRI suggests variability of brain inflammation at early stages after ischemic stroke. Stroke **38**(10), 2733–2737 (2007). https://doi.org/10.1161/strokeaha.107.481788
29. K.E. Sandoval, K.A. Witt, Blood-brain barrier tight junction permeability and ischemic stroke. Neurobiol. Dis. **32**(2), 200–219 (2008). https://doi.org/10.1016/j.nbd.2008.08.005
30. C. Demougeot, M. Van Hoecke, N. Bertrand et al., Cytoprotective efficacy and mechanisms of the liposoluble iron chelator 2,2'-dipyridyl in the rat photothrombotic ischemic stroke model. J. Pharmacol. Exp. Ther. **311**(3), 1080–1087 (2004). https://doi.org/10.1124/jpet.104.072744
31. Q.Z. Tuo, P. Lei, K.A. Jackman et al., Tau-mediated iron export prevents ferroptotic damage after ischemic stroke. Mol. Psychiatr. **22**(11), 1520–1530 (2017). https://doi.org/10.1038/mp.2017.171
32. S.L. Galasso, R.H. Dyck, The role of zinc in cerebral ischemia. Mol. Med. **13**(7–8), 380–387 (2007). https://doi.org/10.2119/2007-00044.Galasso
33. R.D. Palmiter, S.D. Findley, Cloning and functional characterization of a mammalian zinc transporter that confers resistance to zinc. EMBO J. **14**(4), 639–649 (1995). https://doi.org/10.1002/j.1460-2075.1995.tb07042.x
34. C.T. Sheline, M.M. Behrens, D.W. Choi, Zinc-induced cortical neuronal death: contribution of energy failure attributable to loss of NAD(+) and inhibition of glycolysis. J. Neurosci. **20**(9), 3139–3146 (2000). https://doi.org/10.1523/jneurosci.20-09-03139.2000
35. Y. Yamasaki, N. Matsuura, H. Shozuhara et al., Interleukin-1 as a pathogenetic mediator of ischemic brain damage in rats. Stroke **26**(4), 676–681 (1995). https://doi.org/10.1161/01.Str.26.4.676
36. K. Szydlowska, M. Tymianski, Calcium, ischemia and excitotoxicity. Cell Calcium **47**(2), 122–129 (2010). https://doi.org/10.1016/j.ceca.2010.01.003
37. Z. Tang, S. Li, P. Han et al., Pertussis toxin reduces calcium influx to protect ischemic stroke in a middle cerebral artery occlusion model. J. Neurochem. **135**(5), 998–1006 (2015). https://doi.org/10.1111/jnc.13359
38. G. Yu, F. Wu, E.-S. Wang, BQ-869, a novel NMDA receptor antagonist, protects against excitotoxicity and attenuates cerebral ischemic injury in stroke. Int. J. Clin. Exp. Pathol. **8**(2), 1213–1225 (2015)
39. O. Gotoh, T. Asano, T. Koide et al., Ischemic brain edema following occlusion of the middle cerebral artery in the rat. I: The time courses of the brain water, sodium and potassium contents and blood-brain barrier permeability to 125I-albumin. Stroke **16**(1), 101–109 (1985). https://doi.org/10.1161/01.Str.16.1.101
40. U. Ito, K. Ohno, R. Nakamura et al., Brain edema during ischemia and after restoration of blood flow. Measurement of water, sodium, potassium content and plasma protein permeability. Stroke **10**(5), 542–547 (1979). https://doi.org/10.1161/01.str.10.5.542

41. K.A. Hossmann, S. Sakaki, V. Zimmerman, Cation activities in reversible ischemia of the cat brain. Stroke **8**(1), 77–81 (1977). https://doi.org/10.1161/01.str.8.1.77
42. B.S. Jensen, BMS-204352: a potassium channel opener developed for the treatment of stroke. CNS Drug Rev. **8**(4), 353–360 (2002). https://doi.org/10.1111/j.1527-3458.2002.tb00233.x
43. J.Z. Wang, M.V. Vyas, G. Saposnik et al., Incidence and management of seizures after ischemic stroke: systematic review and meta-analysis. Neurology **89**(12), 1220–1228 (2017). https://doi.org/10.1212/WNL.0000000000004407
44. Z. Lei, H. Zhang, Y. Liang et al., Reduced expression of IA channels is associated with post-ischemic seizures. Epilepsy Res. **124**, 40–48 (2016). https://doi.org/10.1016/j.eplepsyres.2016.05.008
45. D.R. Kramer, T. Fujii, I. Ohiorhenuan et al., Interplay between cortical spreading depolarization and seizures. Stereotact. Funct. Neurosurg. **95**(1), 1–5 (2017). https://doi.org/10.1159/000452841
46. A. Zakharov, K. Chernova, G. Burkhanova et al., Segregation of seizures and spreading depolarization across cortical layers. Epilepsia **60**(12), 2386–2397 (2019). https://doi.org/10.1111/epi.16390
47. L.S. Johnson, N. Mattsson, A. Sajadieh et al., Serum potassium is positively associated with stroke and mortality in the large. Population-based malmö preventive project cohort. Stroke **48**(11), 2973–2978 (2017). https://doi.org/10.1161/STROKEAHA.117.018148
48. M. Lai, D. Wang, Z. Lin et al., Small molecule copper and its relative metabolites in serum of cerebral ischemic stroke patients. J. Stroke Cerebrovasc. Dis. **25**(1), 214–219 (2016). https://doi.org/10.1016/j.jstrokecerebrovasdis.2015.09.020
49. M.T. Huuskonen, Q.-Z. Tuo, S. Loppi et al., The copper bis(thiosemicarbazone) complex Cu-II(atsm) is protective against cerebral ischemia through modulation of the inflammatory milieu. Neurotherapeutics **14**(2), 519–532 (2017). https://doi.org/10.1007/s13311-016-0504-9
50. X.Y. Choo, J.R. Liddell, M.T. Huuskonen et al., Cu(atsm) attenuates neuroinflammation. Front. Neurosci. **12**, 668 (2018). https://doi.org/10.3389/fnins.2018.00668
51. J.R. Prohaska, A.A. Gybina, Rat brain iron concentration is lower following perinatal copper deficiency. J. Neurochem. **93**(3), 698–705 (2005). https://doi.org/10.1111/j.1471-4159.2005.03091.x
52. X. Xu, S. Pin, M. Gathinji et al., Aceruloplasminemia: an inherited neurodegenerative disease with impairment of iron homeostasis. Ann. N. Y. Acad. Sci. **1012**, 299–305 (2004). https://doi.org/10.1196/annals.1306.024
53. M.X. Yuan, X.W. Chen, B. Song et al., Characterization of dermal fiber architecture based on X-ray phase contrast microtomography. Nuclear Tech. **43**, 70103 (2020). https://doi.org/10.11889/j.0253-3219.2020.hjs.43.070103
54. J. Hu, P. Li, X. Yin et al., Nondestructive imaging of the internal microstructure of vessels and nerve fibers in rat spinal cord using phase-contrast synchrotron radiation microtomography. J. Synchrotron Radiat. **24**(Pt 2), 482–489 (2017). https://doi.org/10.1107/S1600577517000121
55. M. Zhang, G. Peng, D. Sun et al., Synchrotron radiation imaging is a powerful tool to image brain microvasculature. Med. Phys. **41**, 3 (2014). https://doi.org/10.1118/1.4865784
56. X.Y. Lan, A.G. Li, J. Wang, Bluesky-based fluorescence mapping technology. Nucl. Tech. **42**, 040104 (2019). https://doi.org/10.11889/j.0253-3219.2019.hjs.42.040104. **(in Chinese)**
57. C. Epaule, A. Maksimenko, G. Bastian et al., X-ray microfluorescence for biodistribution studies of nanomedicines. Int. J. Pharm. **531**(1), 343–349 (2017). https://doi.org/10.1016/j.ijpharm.2017.08.106
58. S.T. Kang, T. Wu, Z.H. Chen et al., 3D imaging of rat brain neural network using synchrotron radiation. Nucl. Tech. **43**, 070101 (2020). https://doi.org/10.11889/j.0253-3219.2020.hjs.43.070101. **(in Chinese)**
59. Y. Cao, Y. Zhou, S. Ni et al., Three dimensional quantification of microarchitecture and vessel regeneration by synchrotron radiation microcomputed tomography in a rat model of spinal cord injury. J. Neurotrauma **34**(6), 1187–1199 (2017). https://doi.org/10.1089/neu.2016.4697
60. M.Q. Zhang, D.N. Sun, Y.Y. Xie et al., Three-dimensional visualization of rat brain microvasculature following permanent focal ischaemia by synchrotron radiation. Br. J. Radiol. **87**(1038), 20130670 (2014). https://doi.org/10.1259/bjr.20130670